Supporting Information

$[Ti_8Zr_2O_{12}(COO)_{16}]$ Cluster: An Ideal Inorganic Building Unit for Photoactive Metal−Organic Frameworks

Shuai Yuan,[‡,†] Jun-Sheng Qin,[‡,†] Hai-Qun Xu,[#] Jie Su,[§] Daniel Rossi,[‡] Yuanping Chen,[⊥] Liangliang Zhang,[‡] Christina Lollar,[‡] Qi Wang,[‡] Hai-Long Jiang,*[,#] Dong Hee Son,[‡] Hongyi Xu,[§] Zhehao Huang,*[,§] Xiaodong Zou,[§] and Hong-Cai Zhou*[,‡,∥]

[‡]Department of Chemistry, Texas A&M University, College Station, Texas 77843-3255, United States

[§]Berzelii Centre EXSELENT on Porous Materials and Inorganic and Structural Chemistry, Department of Materials and Environmental Chemistry, Stockholm University, Stockholm 106 91, Sweden

[#]Hefei National Laboratory for Physical Sciences at the Microscale, Collaborative Innovation Center of Suzhou Nano Science and Technology, Department of Chemistry, University of Science and Technology of China, Hefei 230026, P. R. China

[⊥]School of Physics and Optoelectronics, Xiangtan University, Xiangtan 411105, P. R. China

[∥]Department of Materials Science and Engineering, Texas A&M University, College Station, Texas 77843-3003, United States

[†]S.Y. and J.-S.Q. contributed equally to this work.

*Corresponding Author: jianglab@ustc.edu.cn; zhehao.huang@mmk.su.se; zhou@chem.tamu.edu.

Materials and instrumentation. All reagents and solvents were commercially available and used as received. Powder X-ray diffraction (PXRD) was carried out with a Bruker D8-Focus Bragg-Brentano X-ray Powder Diffractometer equipped with a Cu sealed tube (λ = 1.54178 Å) at 40 kV and 40 mA. The UV-Vis absorption spectra were recorded on a Shimadzu UV-2450 spectrophotometer.

Synthesis of [$Ti_8Zr_2O_{12}(MeCOO)_{16}$]. $ZrCl_4$ (50 mg), $Ti(O^iPr)_4$ (0.1 mL), acetic acid (0.5 mL), and acetonitrile (3 mL) were charged in a Pyrex vial. The mixture was heated in a 100 ℃ oven for 24 h. After cooling down to room temperature, colorless crystals were harvested.

Synthesis of [$Ti_8Zr_2O_{12}(EtCOO)_{16}$]. $ZrCl_4$ (50 mg), $Ti(O^iPr)_4$ (0.1 mL), propionic acid (0.5 mL), and acetonitrile (3 mL) were charged in a Pyrex vial. The mixture was heated in a 100 ℃ oven for 24 h. After cooling down to room temperature, colorless crystals were harvested.

Synthesis of [$Ti_8Zr_2O_{12}(PhCOO)_{16}$]. $ZrCl_4$ (50 mg), $Ti(O^iPr)_4$ (0.1 mL), benzoic acid (500 mg), and DMF (1 mL) were charged in a Pyrex vial. The mixture was heated in a 140 ℃ oven for 24 h. After cooling down to room temperature, colorless crystals were harvested.

Synthesis of [$Ti_8Zr_2O_{12}$(p-TolCOO)$_{16}$]. $ZrCl_4$ (50 mg), $Ti(O^iPr)_4$ (0.1 mL), p-toluic acid (500 mg), and DMF (1 mL) were charged in a Pyrex vial. The mixture was heated in a 140 ℃ oven for 24 h. After cooling down to room temperature, colorless crystals were harvested.

Synthesis of [$Ti_8Zr_2O_{12}(PTBB)_{16}$]. $ZrCl_4$ (50 mg), $Ti(O^iPr)_4$ (0.1 mL), p-*t*-butyl benzoic acid (500 mg), and acetonitrile (3 mL) were charged in a Pyrex vial. The mixture was heated in a 100 ℃ oven for 24 h. Colorless crystals were directly collected from hot acetonitrile.

Synthesis of PCN-415. [$Ti_8Zr_2O_{12}(MeCOO)_{16}$] cluster (100 mg), terephthalic acid (800 mg), trifluoroacetic acid (1 mL), and DMF (15 mL) were charged in a Pyrex vial. The mixture was heated in a 140 ℃ oven for 24 h. Alternatively, [$Ti_8Zr_2O_{12}(MeCOO)_{16}$] cluster can be formed *in situ* without separation in the following manner: $ZrCl_4$ (50 mg), $Ti(O^iPr)_4$ (0.1 mL), acetic acid (0.5 mL), and DMF (5 mL) were charged in a Pyrex vial and heated in a 100 ℃ oven for 24 h. Terephthalic acid (800 mg), trifluoroacetic acid (1 mL), and DMF (10 mL) were subsequently added to the mixture. The resulting mixture was heated in a 140 ℃ oven for another 24 h. After cooling down to room temperature, a white crystalline powder was harvested.

Synthesis of PCN-416. $ZrCl_4$ (50 mg), $Ti(O^iPr)_4$ (0.1 mL), acetic acid (0.5 mL), and DMF (5 mL) were charged in a Pyrex vial and heated in a 100 ℃ oven for 24 h. To the mixture was added 2,6-naphthalenedicarboxylic acid (1000 mg), trifluoroacetic acid (1 mL), and DMF (25 mL). The mixture was heated in a 140 ℃ oven for another 24 h. After cooling down to room temperature, a pale yellow crystalline powder was

harvested.

Synthesis of PCN-415-(NH_2)$_{0.3}$. $ZrCl_4$ (50 mg), Ti(O^iPr)$_4$ (0.1 mL), acetic acid (0.5 mL), and DMF (5 mL) were charged in a Pyrex vial and heated in a 100 ℃ oven for 24 h. Terephthalic acid (560 mg), 2-aminoterephthalic acid (262 mg), trifluoroacetic acid (1 mL), and DMF (10 mL) were subsequently added to the mixture. The resulting mixture was heated in a 140 ℃ oven for another 24 h. After cooling down to room temperature, a yellow crystalline powder was harvested. The mole ratio of amino-functionalized linker was determined to be 16% by ^{1}H-NMR.

Synthesis of PCN-415-(NH_2)$_{0.5}$. $ZrCl_4$ (50 mg), Ti(O^iPr)$_4$ (0.1 mL), acetic acid (0.5 mL), and DMF (5 mL) were charged in a Pyrex vial and heated in a 100 ℃ oven for 24 h. Terephthalic acid (400 mg), 2-aminoterephthalic acid (436 mg), trifluoroacetic acid (1 mL), and DMF (10 mL) were subsequently added to the mixture. The resulting mixture was heated in a 140 ℃ oven for another 24 h. After cooling down to room temperature, a yellow crystalline powder was harvested. The mole ratio of amino-functionalized linker was determined to be 35% by ^{1}H-NMR result.

Synthesis of PCN-415-(NH_2)$_{0.7}$. $ZrCl_4$ (50 mg), Ti(O^iPr)$_4$ (0.1 mL), acetic acid (0.5 mL), and DMF (5 mL) were charged in a Pyrex vial and heated in a 100 ℃ oven for 24 h. Terephthalic acid (240 mg), 2-aminoterephthalic acid (610 mg), trifluoroacetic acid (1 mL), and DMF (10 mL) were subsequently added to the mixture. The resulting mixture was heated in a 140 ℃ oven for another 24 h. After cooling down to room temperature, a yellow crystalline powder was harvested. The mole ratio of amino-functionalized linker was determined to be 59% by ^{1}H-NMR result.

Synthesis of PCN-415-NH_2. $ZrCl_4$ (50 mg), Ti(O^iPr)$_4$ (0.1 mL), acetic acid (0.5 mL), and DMF (5 mL) were charged in a Pyrex vial and heated in a 100 ℃ oven for 24 h. 2-Aminoterephthalic acid (872 mg), trifluoroacetic acid (1 mL), and DMF (10 mL) were subsequently added to the mixture. The resulting mixture was heated in a 140 ℃ oven for another 24 h. After cooling down to room temperature, a yellow crystalline powder was harvested.

Synthesis of PCN-415-($2NH_2$)$_{0.5}$. $ZrCl_4$ (50 mg), Ti(O^iPr)$_4$ (0.1 mL), acetic acid (0.5 mL), and DMF (5 mL) were charged in a Pyrex vial and heated in a 100 ℃ oven for 24 h. Terephthalic acid (400 mg), 2,5-diaminoterephthalic acid (472 mg), trifluoroacetic acid (1 mL), and DMF (10 mL) were subsequently added to the mixture. The resulting mixture was heated in a 140 ℃ oven for another 24 h. After cooling down to room temperature, a brown crystalline powder was harvested. The mole ratio of diamino-functionalized linker was determined to be 28% by ^{1}H-NMR result.

Synthesis of PCN-416-($2NH_2$)$_{0.5}$. $ZrCl_4$ (50 mg), Ti(O^iPr)$_4$ (0.1 mL), acetic acid (0.5 mL), and DMF (5 mL) were charged in a Pyrex vial and heated in a 100 ℃ oven for 24 h. To the mixture was added 2,6-naphthalenedicarboxylic acid (500 mg), 4,8-diaminonaphthalene-2,6-dicarboxylic acid (570 mg), trifluoroacetic acid (1 mL),

and DMF (25 mL). The mixture was heated in a 140 ℃ oven for another 24 h. After cooling down to room temperature, a pale yellow crystalline powder was harvested. The mole ratio of diamino-functionalized linker was determined to be 32% by ^{1}H-NMR result.

N_2 sorption isotherm. Before gas sorption experiments, as-synthesized samples were washed with DMF and immersed in acetone for 3 days, during which the solvent was decanted and freshly replenished three times. The solvent was removed under vacuum at 100 ^{o}C, yielding porous material. Gas sorption measurements were then conducted using a Micrometritics ASAP 2020 system.

^{1}H NMR spectroscopy. For ^{1}H NMR spectroscopy, the activated samples (around 5 mg) were dissolved by saturated Na_2CO_3 aqueous solution (1 mL), neutralized by 10 M HCl aqueous solution, and dried in a 100 ^{o}C oven. The solid was dissolved in ~0.5 mL DMSO-d_6 for ^{1}H NMR analysis. ^{1}H NMR data were collected on a Mercury 300 spectrometer.

Scanning electron microscopic (SEM) and transmission electron microscopic (TEM) analysis. Images and analyses of SEM/EDX were taken by FEI Quanta 600 FE-SEM. The Quanta 600 FEG is a field emission scanning electron microscope capable of generating and collecting high-resolution and low-vacuum images. It is equipped with a motorized x-y-z-tilt-rotate stage, providing the following movements: $x = y$ = 150 mm (motorized); z = 65 mm (motorized); Tilt +70 degrees to –5 degrees (motorized); Source: Field emission gun assembly with Schottky emitter source. Voltage: 200 V to 30 kV. Beam Current: >100 nA. Transmission electron microscopy (TEM) experiments were conducted on a FEI Tecnai G2 F20 ST microscope (America) operated at 200 kV.

ICP-MS Analysis. Samples were prepared in triplicate with weights of around 3 mg. Each sample was dissolved in J.T. Baker Ultrex® II Ultrapure 70% nitric acid at 70 ^{o}C for 12 hours. Samples were then diluted to 150x in 1% nitric acid and 18.2 MΩ water from a Millipore Milli-Q® water purification system. Calibration standards were prepared from certified reference standards from RICCA Chemical Company. Samples were further analyzed with a Perkin Elmer NexION® 300D ICP-MS. Resulting calibration curves have minimum R^2 = 0.9999. Additionally, in order to maintain accuracy, quality control samples from certified reference standards and internal standards were utilized. The individual results of the triplicate samples were averaged to determine the metal ratios.

Single Crystal X-ray Crystallography. All crystals were taken from the mother liquid without further treatment, transferred to oil and mounted into a loop for single crystal X-ray data collection. Diffraction was measured on a Bruker D8 Venture or D8 Quest diffractometer equipped with a Mo-Kα sealed-tube X-ray source (λ = 0.71073 Å, graphite monochromated) at low temperature device (100 K). The data frames

were recorded using the program *APEX2* and processed using the program *SAINT* routine within *APEX2*.[1] The data were corrected for absorption and beam corrections based on the multi-scan technique as implemented in *SADABS*.[2] The structures were solved by direct methods using *OLEX2* software packages, and refined by full-matrix least-squares on F^2 using *SHELXL* software.[3]

For the refinements, all non-hydrogen atoms were refined with anisotropic displacement parameters. Those with enormous thermal ellipsoids were refined with the help of *EADP* restrains on each ligand to clear the warnings about non-positive definite matrices. For $[Ti_8Zr_2O_{12}(RCOO)_{16}]$ (R = Me, p-Tol and PTBB), the solvent mask procedure in *OLEX2* was employed,[4] because the solvent molecule can be neither identified nor modeled. For $[Ti_8Zr_2O_{12}(RCOO)_{16}]$ (R = PTBB), the FragmentDB constrains in *OLEX2* was adopted for the refinement of *tert*-Butyl-C fragment.[5]

It should be noted that the crystal quality of $[Ti_8Zr_2O_{12}(RCOO)_{16}]$ (R = PTBB) is not good because it is directly taken from hot acetonitrile. On the one hand, the acetonitrile molecules on the surface of crystals would be rapidly evaporated, leading to the formation of crack in the crystal. On the other hand, the excessive *p*-*t*-butylbenzoic acid in the hot acetonitrile would be remained on the surface of crystals with the leaving of acetonitrile. In addition, the Mo-Kα sealed-tube as X-ray source for the single crystal diffraction makes a relatively weaker diffraction data. However, the significant Fourier peaks were clear to construct the *p*-*t*-butylbenzoic acid ligands coordinated on the Ti_8Zr_2 clusters. Also the Ti_8Zr_2 clusters are isostructural to coordinate with different terminal carboxylic acids. We believe this proposed structure is well-determined for this compound.

Continuous Rotation electron diffraction (*c*RED) collection. The crystal sizes of PCN-415 and -416 are less than 1 μm, which is too small to be solved by single crystal X-ray diffraction. Therefore continuous rotation electron diffraction (*c*RED) was applied for solving and refining their structures. Samples of as-made PCN-415 and -416 for TEM investigations were dispersed in acetone. A droplet of the suspension was transferred onto a carbon-coated copper grid. *c*RED data collection was performed on a JEOL JEM2100 microscope and operated at 200 kV (Cs 1.0 mm, point resolution 0.23 nm). Images and electron diffraction patterns were recorded with a Timepix pixel detector QTPX-262k (512 x 512 pixels, pixel size 55 μm, Amsterdam Sci. Ins.) under low-dose conditions. The data were collected using the software *cREDCollection*.[6] A single-tilt tomography sample holder was used for the data collection, which could tilt from -70 ° to +70 ° in the TEM. The area for *c*RED data collection was selected using the selected area aperture with about 1.0 μm in diameter. The speed of goniometer tilt was 0.10 ° - 0.45 ° s^{-1}, and the exposure time was 0.1 - 0.5 s per frame. Ultrafast 3D *c*RED data collection was carried out in 17 s – 3 min to

minimize the beam damage and to maximize the data quality. The data was processed by using XDS package,[7] and two data sets were merged for PCN-416. The *c*RED data resolution reached 0.75 Å for PCN-415 and 1.05 Å for PCN-416. The data completeness is 99.0 % for PCN-415 and 100.0% for PCN-416.

The unit cell and possible space groups were easily determined from the 3D reciprocal lattice of PCN-415 and -416 reconstructed using the *RED processing software*.[6] They crystallize in *I*-centered tetragonal unit cells with cell parameters of a = 14.38 Å and c = 26.98 Å for PCN-415, and a = 16.50 Å and c = 29.95 Å for PCN-416. The reflection conditions of PCN-415 and -416 were clearly deduced from the 2D slices cut from the reconstructed 3D reciprocal lattice. Considering the reflection conditions and the symmetry of the linkers, *I*4/*mmm* and *I*-42*m* space groups were chosen for PCN-415 and -416, respectively.

The framework structures were determined by direct methods using the program Shelx-2014.[8] For PCN-415, all the atoms were directly found. For PCN-416, all the Zr, Ti, O atoms, and 16 C atoms were directly found, and the remaining two C atoms were located from difference Fourier maps. The final refinement was done by using Shelxl-2014 with only soft restrains on the ligand molecules and based on the kinematic intensities. The data converged to R1 = 0.233 for PCN-415 and 0.258 for PCN-416. The high R1 value is mainly caused by the dynamical effects that make the *c*RED intensities deviating from the kinematic intensities. The details of data collection and refinement are summarized in Tables S3.

Rietveld refinement. The structures of PCN-415 and -416 obtained from *c*RED data were further refined against synchrotron powder X-ray diffraction (PXRD) data (λ = 0.72768 Å). Synchrotron powder X-ray diffraction (PXRD) was collected on the beamline 17-BM at the Advanced Photon Source, Argonne National Laboratory. Rietveld refinement[9] was performed using TOPAS Academic V4.1.

For PCN-415, the background was fitted with an 11th order Chebychev polynomial. The refinement was conducted using a Pearson VII type peak profile function, followed by refinement of the unit cell and zero-shift. Soft-restrains were applied to the Ti-O and Zr-O distances by 2.00 Å and 2.20 Å, respectively. Rigid bodies were applied on the ligands. The guest species in the cages could not be located due to their partial occupancies and low symmetry. Instead, five oxygen atoms were added at random positions inside the cages to compensate for the contributions of the guest species, and refined subsequently. Finally, R-value was converged to R_p= 0.03243, R_{wp}= 0.04954, R_{exp}= 0.03572, and GOF= 1.387.

For PCN-416, the background was fitted with a 14th order Chebychev polynomial. The refinement was conducted using a Pearson VII type peak profile function, followed by refinement of the unit cell and zero-shift. Soft-restrains were applied to the Ti-O and Zr-O distances by 2.00 Å and 2.20 Å, respectively. Rigid bodies were applied on the ligands. The guest species in the cages could not be

located owing to their partial occupancies and low symmetry. Instead, six oxygen atoms were added at random positions inside the cages to compensate for the contributions of the guest species, and refined subsequently. Finally, R-value was converged to R_p= 0.03840, R_{wp}= 0.05313, R_{exp}= 0.04694, and GOF= 1.132. The details of PXRD data collection and refinement are summarized in Tables S4.

EPR analysis. Electron Paramagnetic Resonance (EPR) measurement was conducted on a Bruker Elexsys II E500 EPR spectrometer equipped with a Bruker ER4131VT variable-temperature unit. About 10 mg of PCN-415-NH_2 sample and 1 mL methanol were sealed in a 1.5 mm quartz tube. The tube was kept sealed throughout the measurement. The spectra of samples before and after light irradiation were measured. The spectra were recorded at 75 K with 0.6325 mW microwave power and a modulation amplitude of 5.0 G. The microwave frequency was set at 9.374 GHz. The field was centered at 3500G with a sweep width of 2000G. Each spectrum was integrated from 60 scans.

Transient absorption measurement. Transient absorption was measured in the pump−probe setup monitoring the change of absorption peak at 580 nm after band gap excitation. The 400 nm pump was generated from 100 fs, 800 nm wavelength, Ti-sapphire laser operating at 82 MHz by second harmonic generation. Several μJ of a 800 nm beam were focused onto the translating CaF_2 window to generate a stable supercontinuum, which was used as the probe beam. The probe beam centered at 580 nm was selected with the bandwidth (fwhm) of ~10 nm before the sample using a chirp compensating prism pair and a spatial filter. The instrument-limited response time was ~80 fs. In a typical experiment 20 mg MOF was dispersed in acetonitrile (20 mL) and sonicated for 30 min. In order to separate large particles, the suspension was then centrifuged for 20 min at 6000 rpm. The supernatant was placed in a 2 mm stirred quartz cuvette for the measurements. Multiexponential fitting to this asymptotic recovery gives rise to two characteristic time constants, τ_1 = 1 ps and τ_2 = 80 ps. Notably, the nearly perfect parallelism between the asymptote and the ΔOD = 0 line suggests that the eventual recovery to ΔOD = 0 features an extremely long lifetime (τ_3), probably a few nanoseconds or longer.

Photocatalytic hydrogen production. The photocatalytic hydrogen production experiments were carried out in a 160 mL optical reaction vessel with stirring at ambient temperature using a 300 W Xe lamp equipped with a UV cut-off filter (λ > 380 nm). In the reaction vessel, 5 mg of the MOF catalyst was dispersed in 28 mL acetonitrile with 0.2 mL deionized water, 2 mL triethanolamine (TEOA) as a sacrificial reagent, and ~50 μg of Pt nanoparticles as co-catalyst. The suspension was stirred and purged with nitrogen for ~60 min to remove air. Hydrogen gas was measured by gas chromatography (Shimadzu GC-2014, argon as a carrier gas) using a thermal conductivity detector (TCD).

DFT calculations. First-principles calculations were based on the density functional

theory (DFT) as implemented in the Vienna Ab-initio Simulation Package[10]. The core-valence interactions were described by projector augmented-wave (PAW) potentials within the Perdew-Burke-Ernzerhof (PBE) approximation for the exchange-correlation energy[11]. Plane waves with a kinetic energy cutoff of 500 eV were used as the basis set. We used the conjugate gradient method to optimize the atomic positions, and the energy convergence criterion between two consecutive steps was 10^{-5} eV. The maximum allowed force on the atoms is 10^{-3} eV/Å. Note that the DFT predictions are useful for a quantitative comparison between themselves. The absolute band gap energy, however, is underestimated when compared to the experimentally measured optical band gaps. This discrepancy in the band gap is a classic occurrence in DFT ground state predictions which arises from the approximations in the exchange-correlation. In addition, defects in MOFs may change the band gap, but the effect of which is difficult to estimate in DFT calculations.

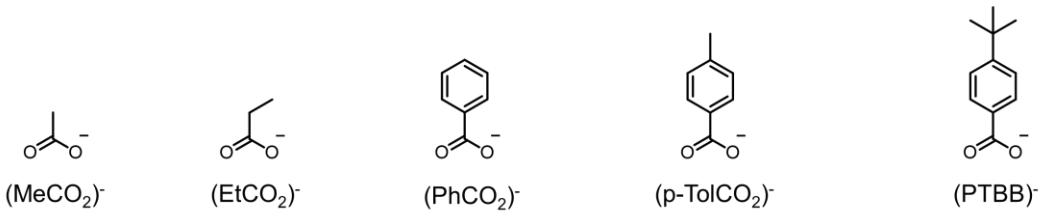

Figure S1. The terminal carboxylates employed in this work to build $[Ti_8Zr_2O_{12}(RCOO)_{16}]$ clusters.

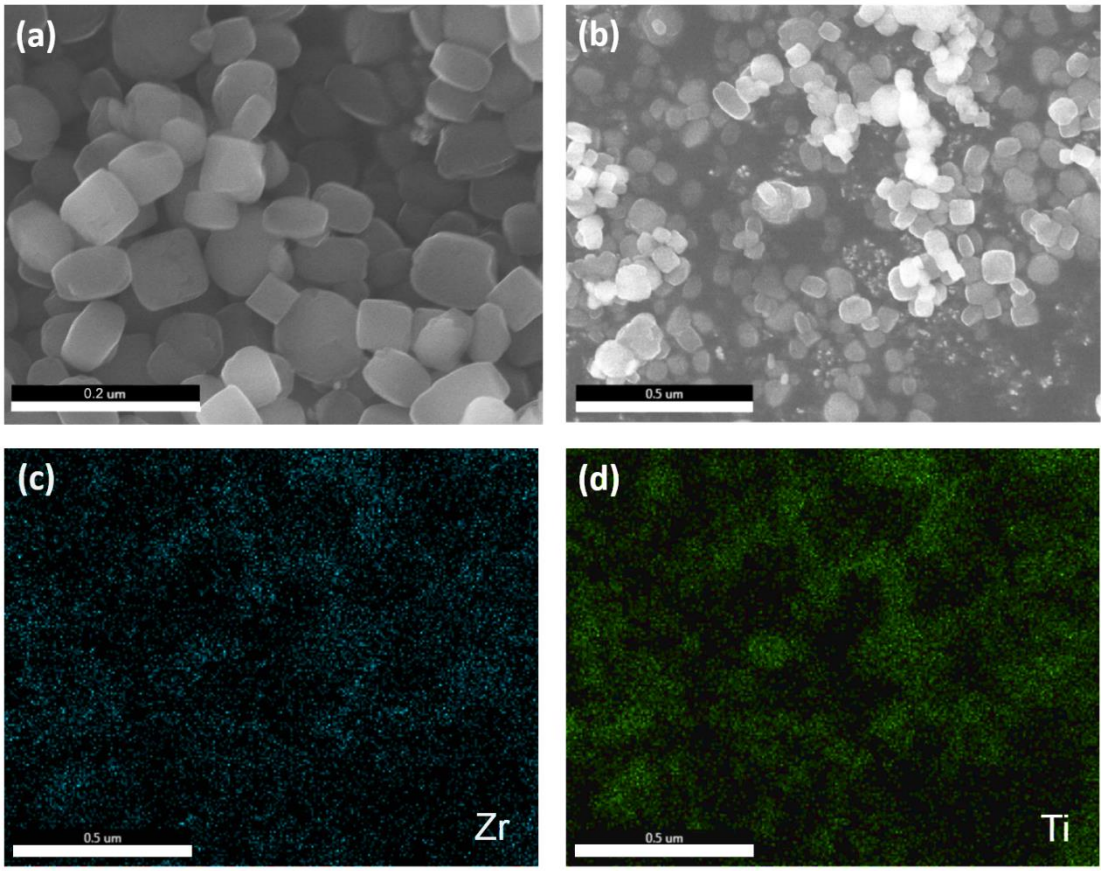

Figure S2. The SEM images (a and b) and corresponding elemental mapping (c and d) of PCN-415.

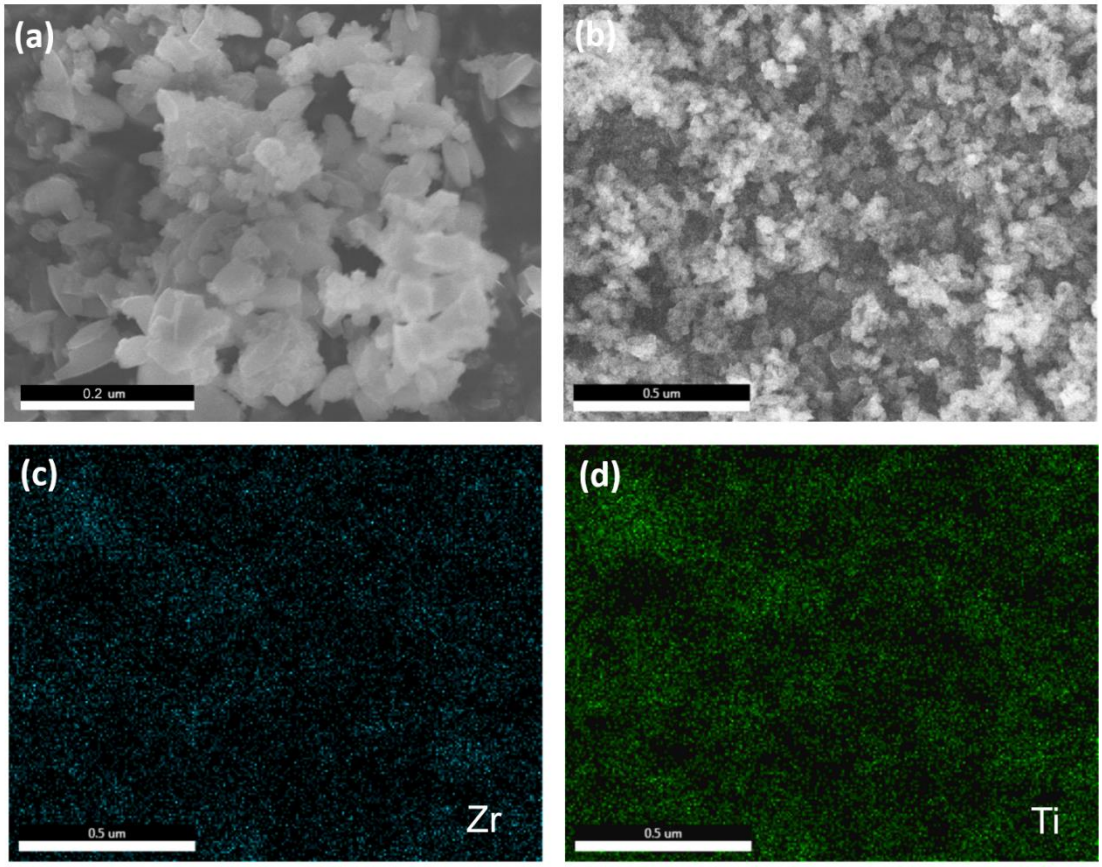

Figure S3. The SEM images (a and b) and corresponding elemental mapping (c and d) of PCN-416.

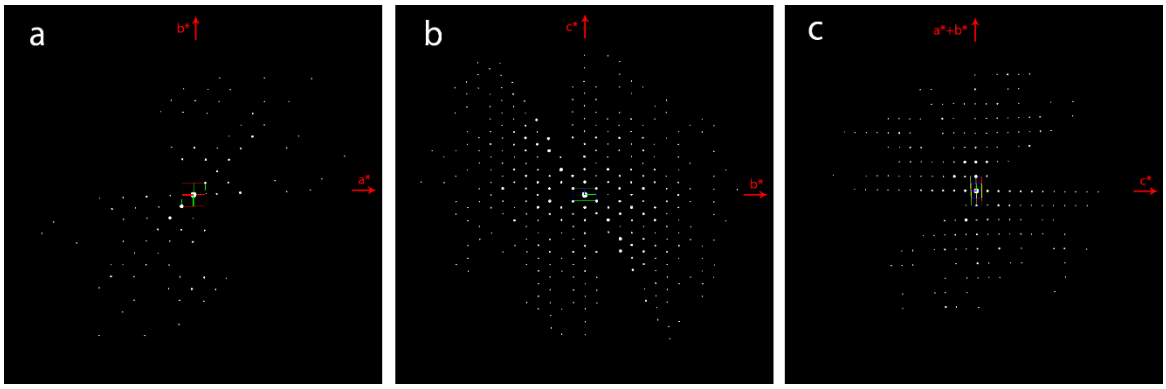

Figure S4. 2D slices cut from the reconstructed 3D reciprocal lattice of PCN-415 showing the (a) *hk*0, (b) 0*kl*, and (c) *hhl* plane.

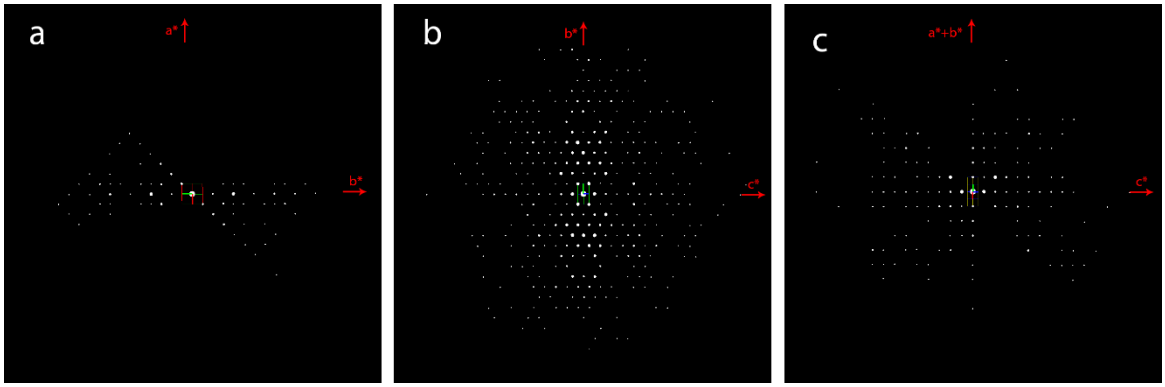

Figure S5. 2D slices cut from the reconstructed 3D reciprocal lattice of PCN-416 showing the (a) *hk*0, (b) 0*kl*, and (c) *hhl* plane.

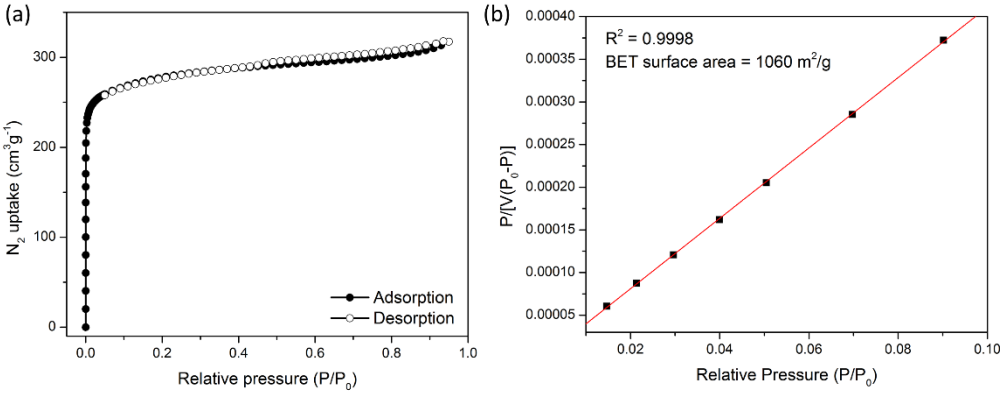

Figure S6. (a) N_2 adsorption-desorption isotherms and (b) BET surface area calculation of PCN-415.

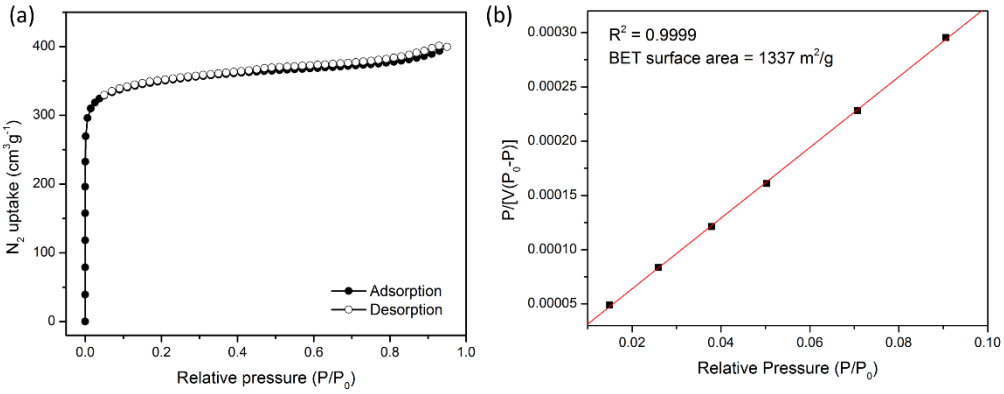

Figure S7. (a) N_2 adsorption-desorption isotherms and (b) BET surface area calculation of PCN-416.

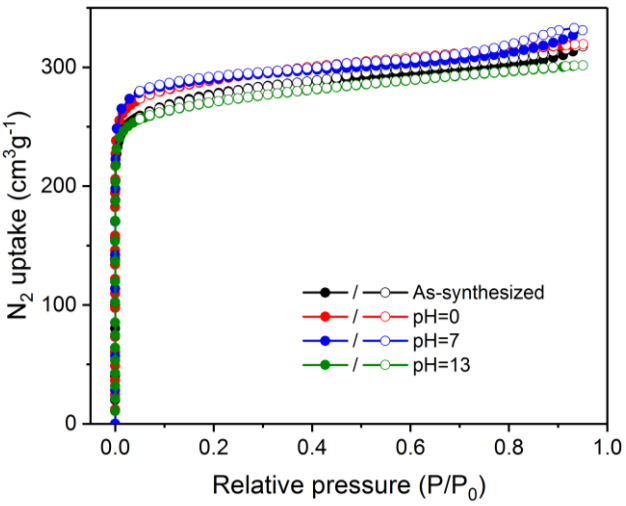

Figure S8. N_2 adsorption-desorption isotherms of PCN-415 after immersion in aqueous solutions with different pH values at room temperature for 24 h.

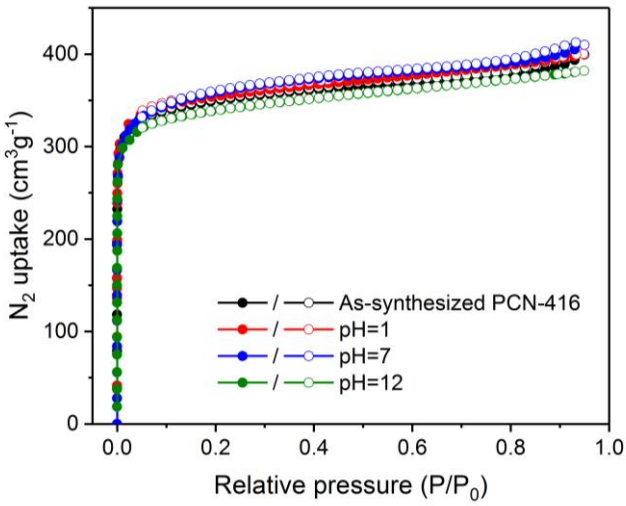

Figure S9. N_2 adsorption-desorption isotherms of PCN-416 after immersion in aqueous solutions with different pH values at room temperature for 24 h.

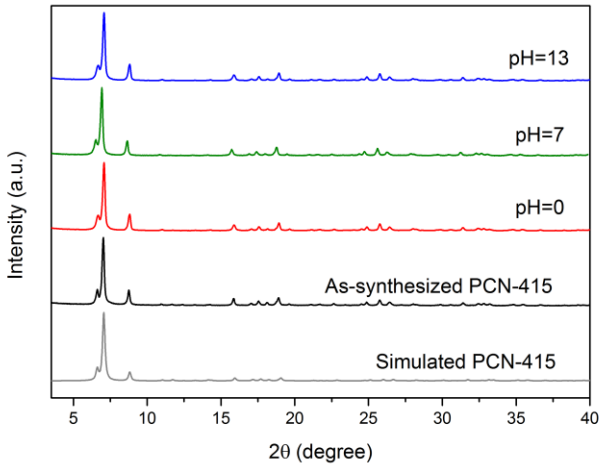

Figure S10. PXRD patterns of PCN-415 before and after immersion in aqueous solutions with different pH values at room temperature for 72 h.

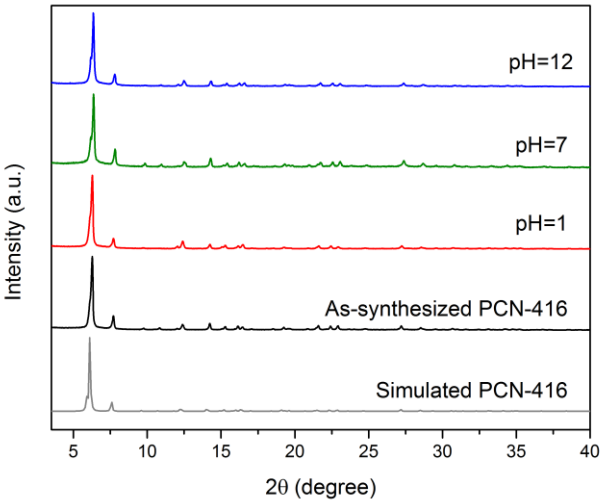

Figure S11. PXRD patterns of PCN-416 before and after immersion in aqueous solutions with different pH values at room temperature for 24 h.

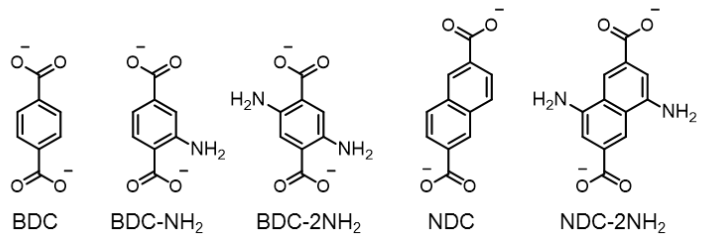

Figure S12. The linkers employed in this work: BDC, NDC, and their derivatives.

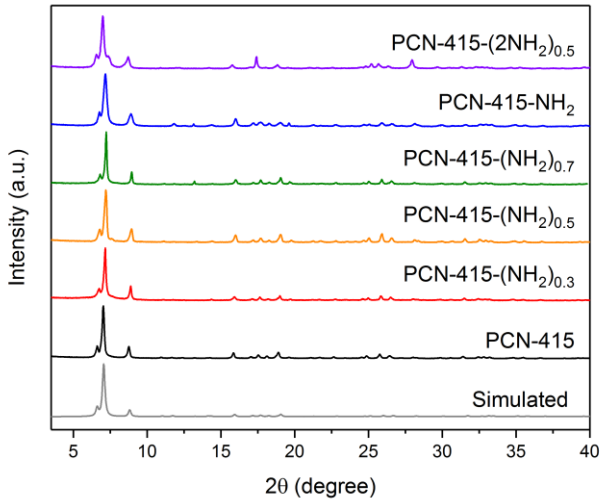

Figure S13. PXRD patterns of PCN-415 and its –NH_2 functionalized derivatives.

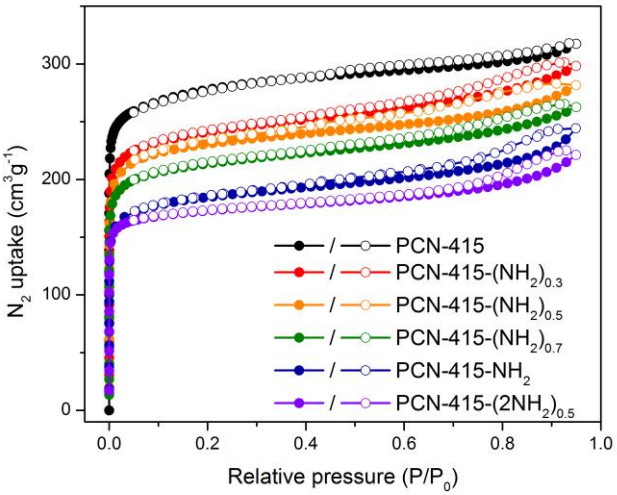

Figure S14. N_2 adsorption-desorption isotherms of PCN-415 and its –NH_2 functionalized derivatives.

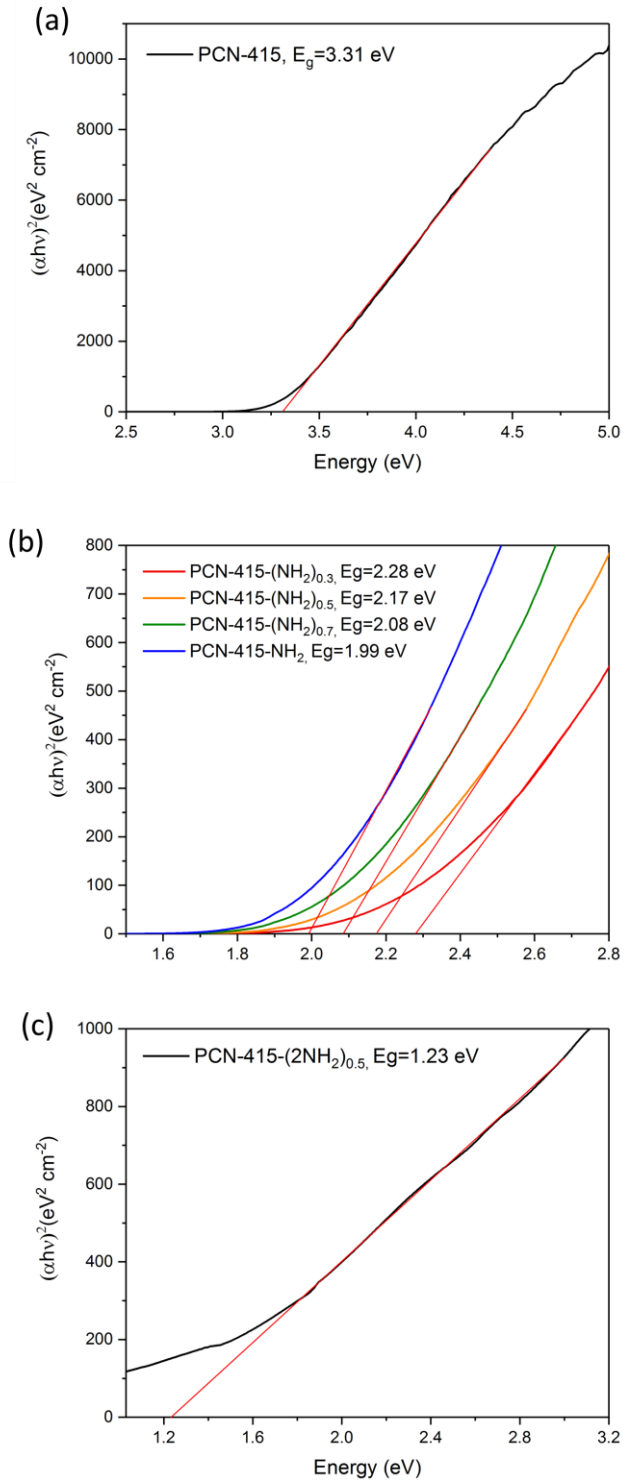

Figure S15. Calculations of band-gaps for PCN-415 and its amine functionalized derivatives using Tauc plots.

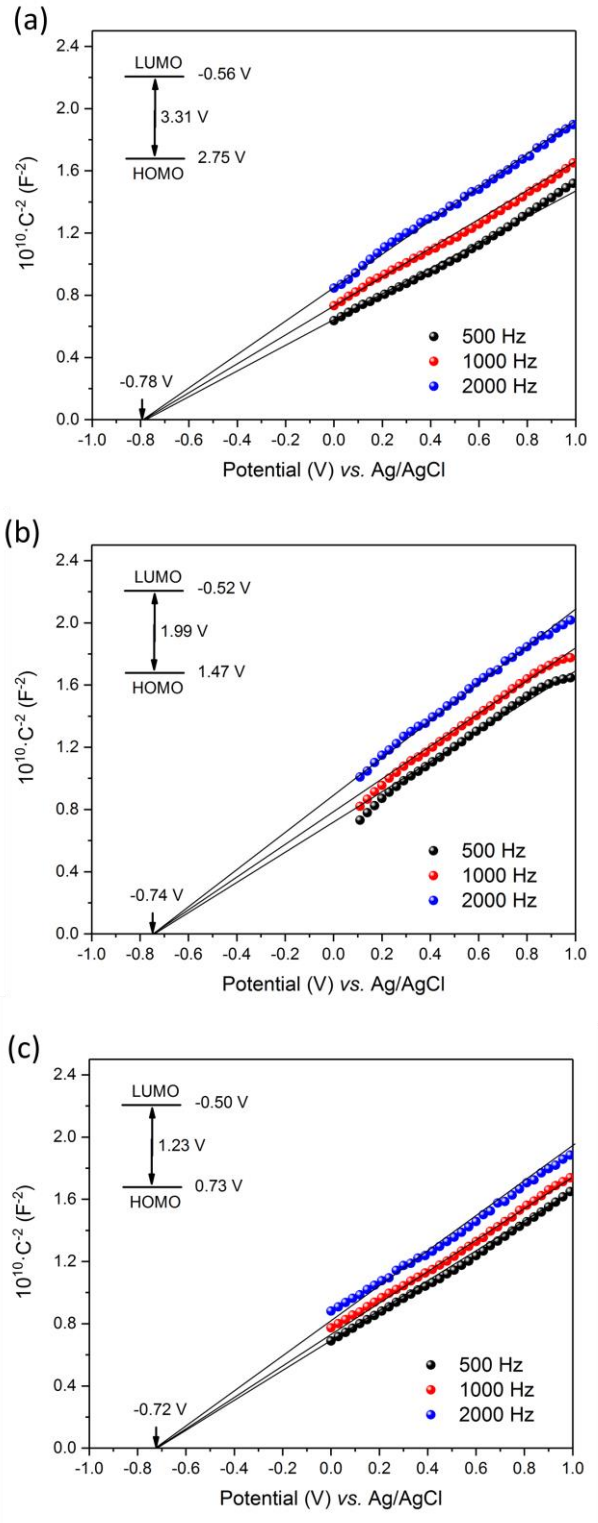

Figure S16. The Mott-Schottky plots of (a) PCN-415, (b) PCN-415-NH_2, and (c) PCN-415-$(2NH_2)_{0.5}$.

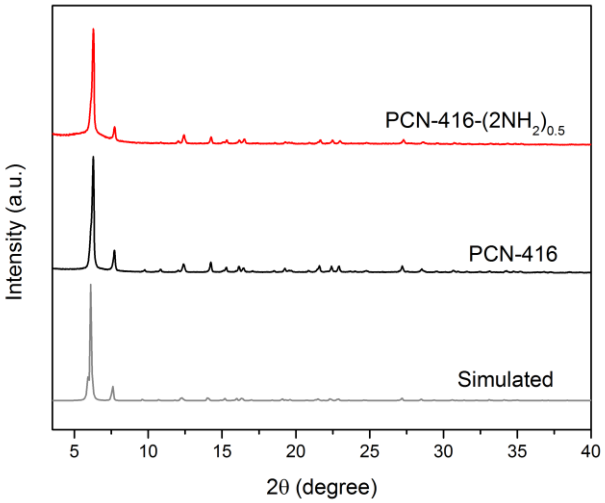

Figure S17. PXRD patterns of PCN-416 and PCN-416-$(2NH_2)_{0.5}$.

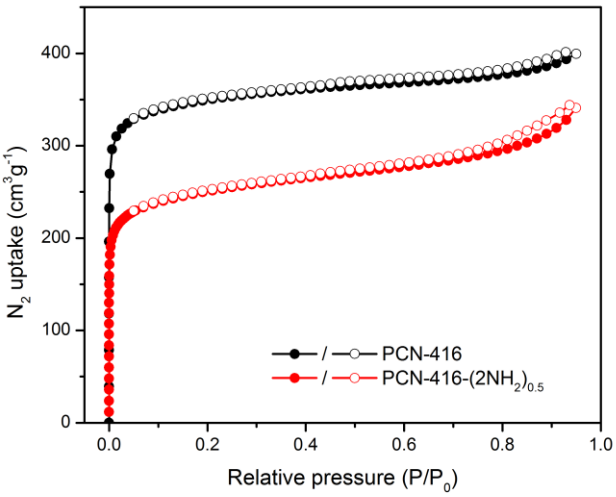

Figure S18. N_2 adsorption-desorption isotherms of PCN-416 and PCN-416-$(2NH_2)_{0.5}$.

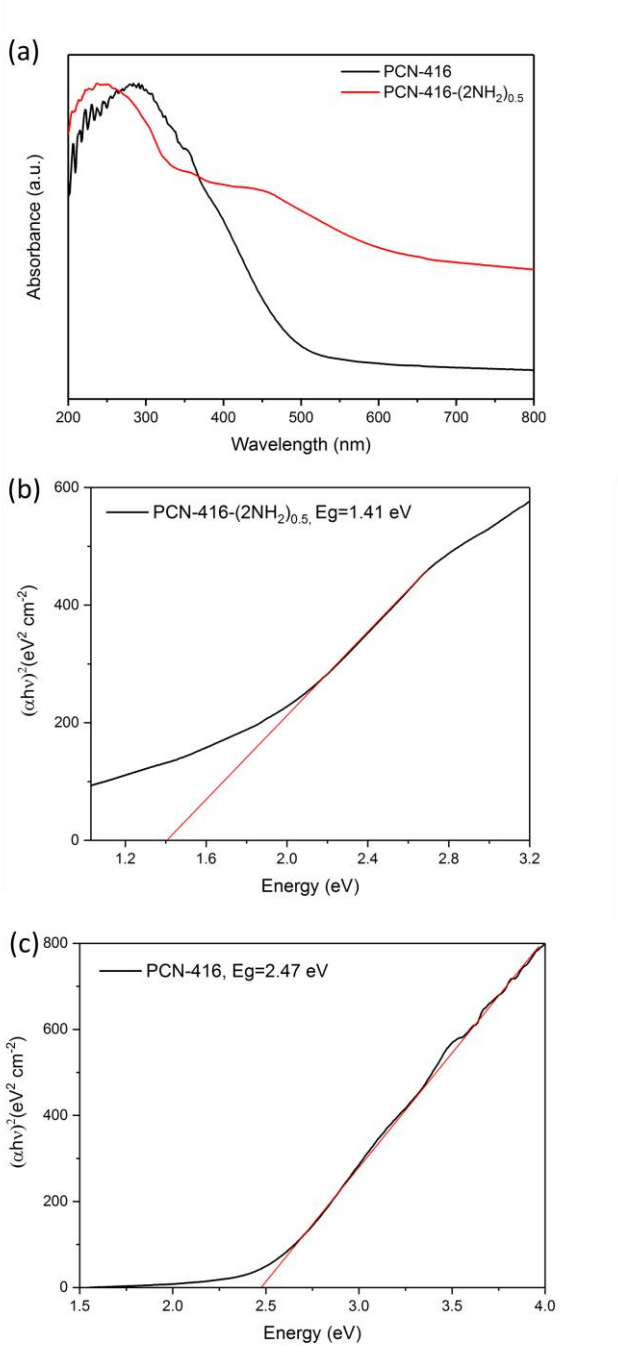

Figure S19. (a) The UV-Vis spectra of PCN-416 and PCN-416-$(2NH_2)_{0.5}$. Calculations of band-gaps for (b) PCN-416 and (c) PCN-416-$(2NH_2)_{0.5}$ using Tauc plots.

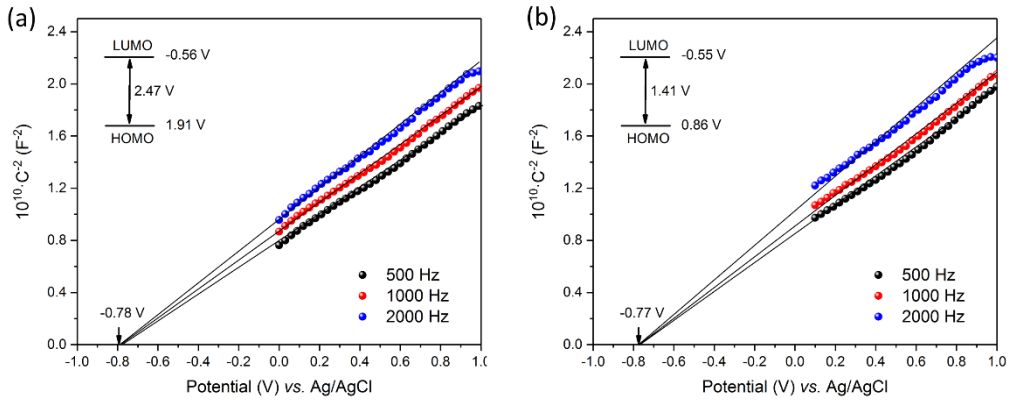

Figure S20. The Mott-Schottky plots of (a) PCN-416 and (b) PCN-416-$(2NH_2)_{0.5}$.

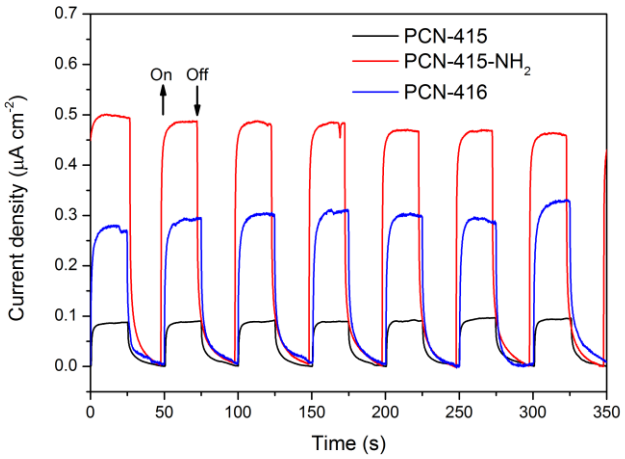

Figure S21. The photocurrent responses of PCN-415, -415-NH_2, and -416.

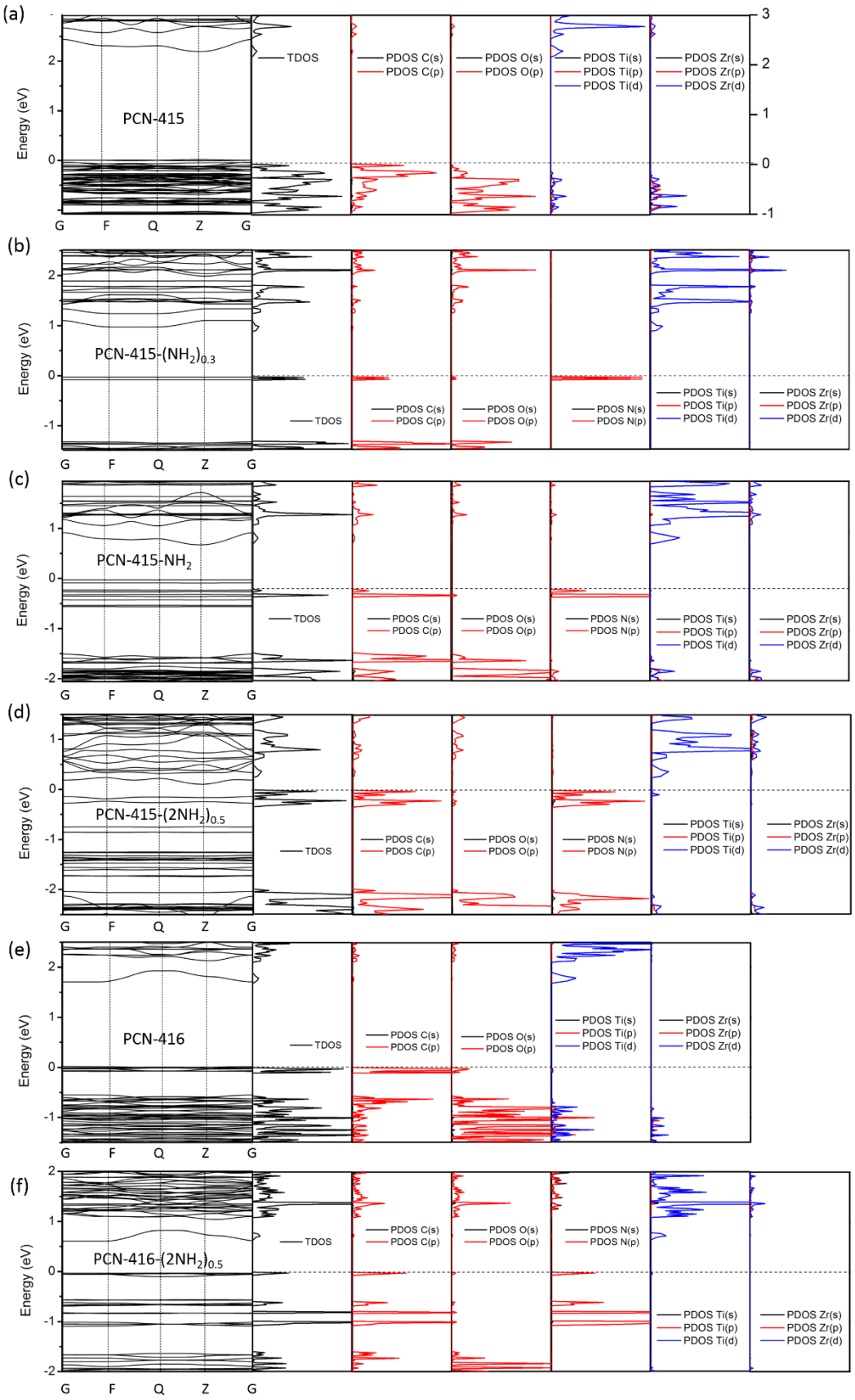

Figure S22. DFT calculated band structures for PCN-415, PCN-416 and their derivatives.

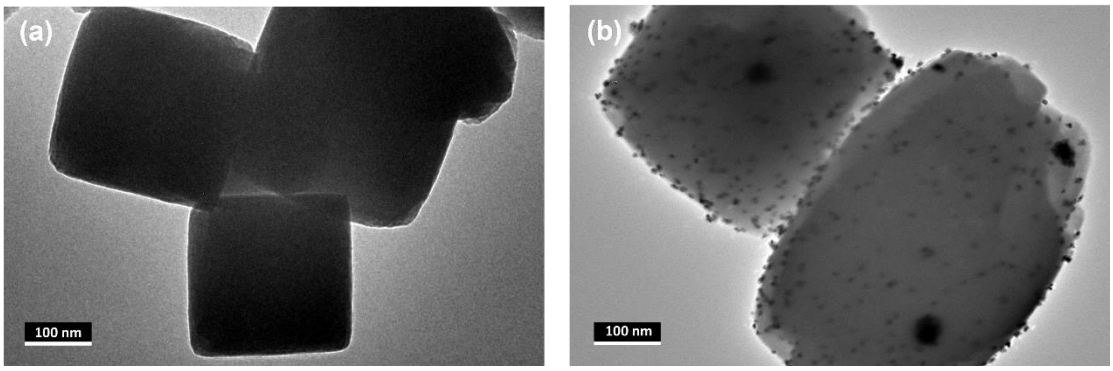

Figure S23. The TEM images of PCN-415 (a) before and (b) after Pt loading.

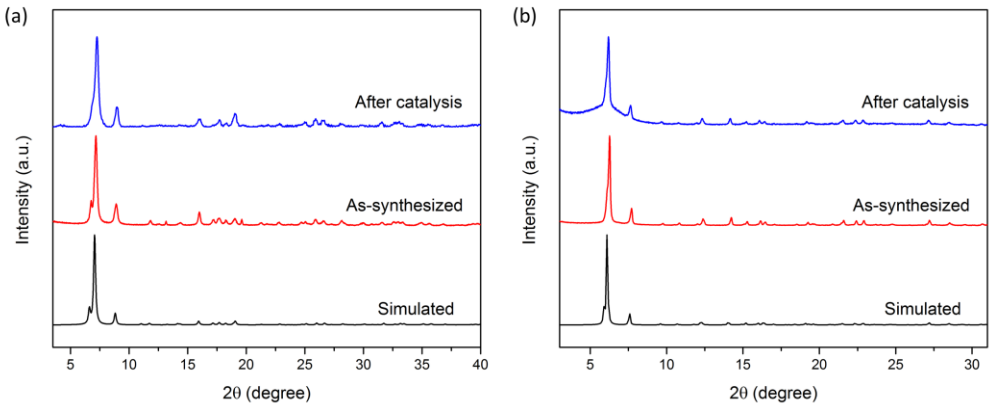

Figure S24. The PXRD patterns of (a) PCN-415-NH_2 and (b) PCN-416 before and after photocatalytic hydrogen generation.

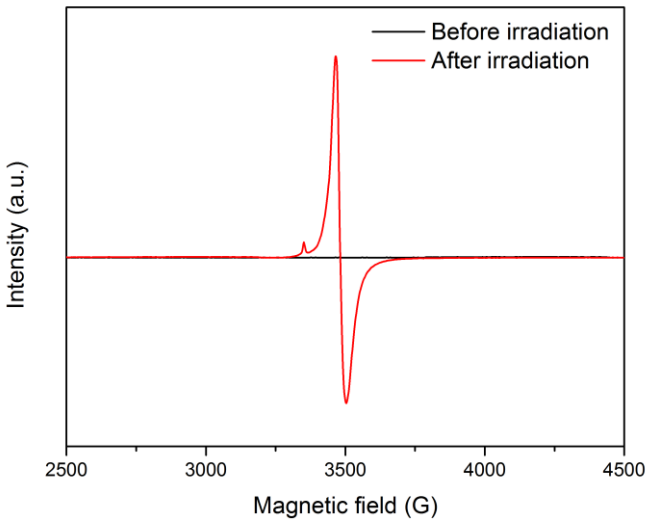

Figure S25. The EPR spectra of PCN-415-NH_2 before and after light irradiation.

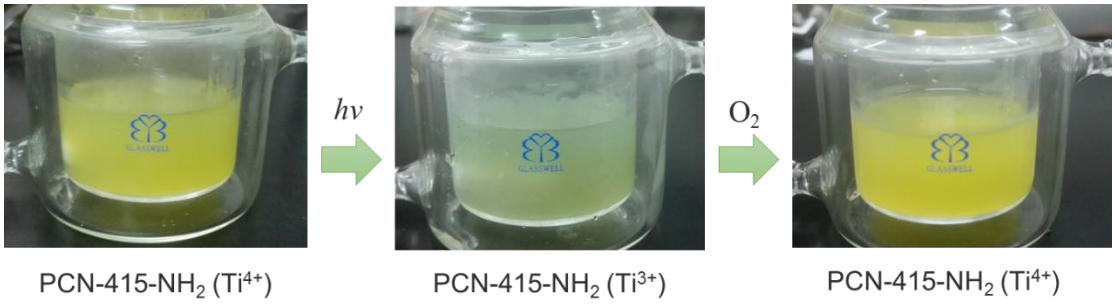

Figure S26. The color change of the reaction suspension upon light irradiation in the presence of N_2 and quickly back upon exposure to O_2.

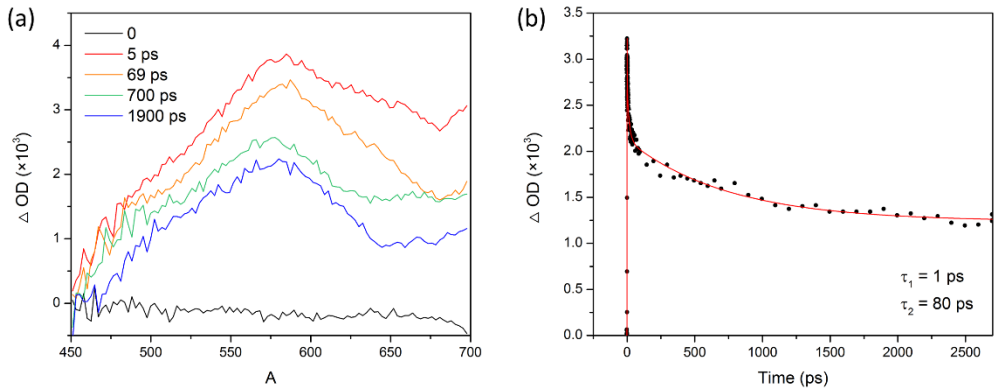

Figure S27. Transient absorption spectroscopy. (a) Differential transient absorption spectra for PCN-415-NH_2 upon excitation at 400 nm; (b) TA kinetics of PCN-415-NH_2 taken at the probing wavelength of 580 nm.

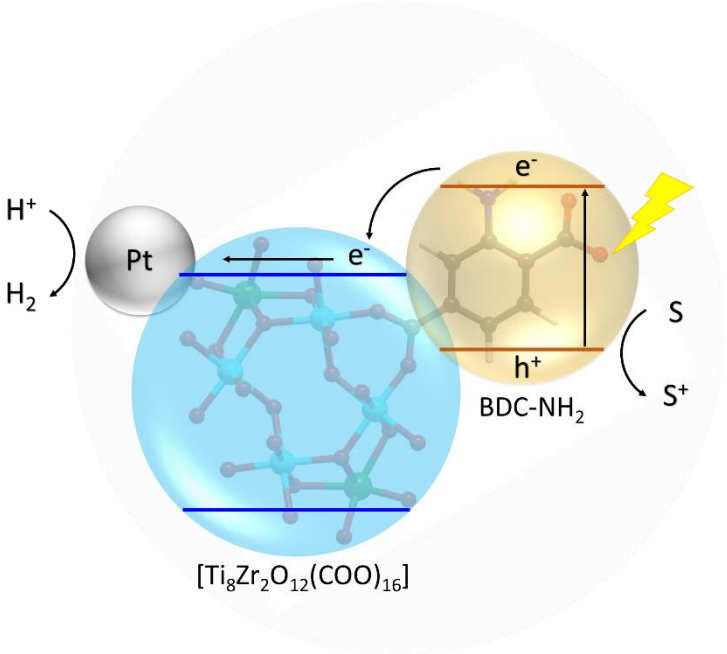

Figure S28. Proposed mechanism of the hydrogen generation reaction catalyzed by Pt@PCN-415-NH_2.

Table S1. Crystal data and structure refinements for $[Ti_8Zr_2O_{12}(RCOO)_{16}]$ clusters

	R = Me	R = Et	R = Ph
CCDC	1568410	1568409	1568406
Empirical formula	$C_{288}H_{432}N_{48}O_{264}Ti_{48}Zr_{12}$	$C_{48}H_{80}O_{44}Ti_8Zr_2$	$C_{224}H_{160}O_{88}Ti_{16}Zr_4$
M_w	12184.63	1926.76	5390.79
Color/Shape	Colorless block	Colorless block	Colorless block
Crystal system	Cubic	Triclinic	Monoclinic
Space group	*Im*-3*m*	*P*-1	$P2_1/n$
a (Å)	24.260(4)	12.064(3)	14.896(4)
b (Å)	24.260(4)	13.543(3)	24.070(6)
c (Å)	24.260(4)	13.806(3)	15.304(4)
α (deg)	90	104.331(3)	90
β (deg)	90	109.519(3)	91.287(4)
γ (deg)	90	110.620(3)	90
V (Å^3)	14279(7)	1811.3(8)	5486(2)
Z	1	1	1
T (K)	296(2)	293(2)	296(2)
Wavelength (Å)	0.71073 (MoK_α)	0.71073 (MoK_α)	0.71073 (MoK_α)
D_c (Mg m^{-3})	1.417	1.766	1.632
Abs. coeff. (mm^{-1})	0.925	1.206	0.824
R_{int}	0.0440	0.0488	0.0793
F(000)	6144	976	2720
reflns collected	92448	23285	48548
Independent reflns	1969	9407	12788
GOF on F^2	1.137	1.031	1.026
R_1 [$I > 2\sigma(I)$][a]	0.0137	0.0425	0.0474
wR_2 [$I > 2\sigma(I)$][a]	0.0514	0.0887	0.0987
R_1 (all data)[b]	0.0219	0.0667	0.0773
wR_2 (all data)[b]	0.0530	0.0998	0.1108

	R = p-Tol	R = PTBB
CCDC	1568407	1568408
Empirical formula	$C_{134}H_{126}N_2O_{46}Ti_8Zr_2$	$C_{176}H_{209}O_{44}Ti_8Zr_2$
M_w	3066.00	3594.06
Color/Shape	Colorless block	Colorless block
Crystal system	Trigonal	Monoclinic
Space group	*R*-3*c*	$P2_1$
a (Å)	32.890(7)	15.818(12)
b (Å)	32.890(7)	35.48(3)
c (Å)	73.485(15)	18.356(14)
α (deg)	90	90
β (deg)	90	108.901(12)
γ (deg)	120	90
V (Å^3)	68844(31)	9745(13)
Z	18	2
T (K)	296(2)	296(2)
Wavelength (Å)	0.71073 (MoK$_\alpha$)	0.71073 (MoK$_\alpha$)
D_c (Mg m^{-3})	1.331	1.225
Abs. coeff. (mm^{-1})	0.601	0.480
R_{int}	0.1043	0.3746
F(000)	28224	3746
reflns collected	118987	82153
Independent reflns	17545	28257
GOF on F^2	1.006	0.967
R_1 [$I > 2\sigma(I)$][a]	0.0586	0.1497
wR_2 [$I > 2\sigma(I)$][a]	0.1409	0.3343
R_1 (all data)[b]	0.1289	0.3537
wR_2 (all data)[b]	0.1828	0.4518

[a] $R_1 = \Sigma||F_o| - |F_c||/\Sigma|F_o|$.

[b] $wR_2 = |\Sigma w(|F_o|^2 - |F_c|^2)|/\Sigma|w(F_o^2)^2|^{1/2}$.

Table S2. Crystallographic details for the refinement of PCN-415 and -416 against the *c*RED data. *

Name	**PCN-415**	**PCN-416**
Wavelength (Å)	0.0251	0.0251
Program	Shelxl-2014	Shelxl-2014
Tilt range	-31.9°-43.0°	-60.4 °-40.7°
Total number of frames	340	458
Space group	*I*4/*mmm*	*I*-42*m*
Unit cell parameter	*a*=14.4Å, *c*=26.4 Å	*a*=16.7Å, *c*=30.1 Å
Resolution (Å)	0.75	1.05
Completeness	99.0	100.0
No. unique reflections	1970	1918
No. observed reflections (I > 2 sigma(I))	1384	912
R1 (I > 2 sigma(I))	0.233	0.258
R1 (all reflections)	0.248	0.317
Goof	2.01	1.50

* Hydrogen atoms were not included in the refinement.

Table S3. Crystallographic data, powder X-ray collection conditions, and Rietveld refinement results of PCN-415 and -416.

Name	**PCN-415**	**PCN-416**
Chemical formula	$C_{32}H_{16}O_{37.08}Ti_4Zr$	$C_{48}H_{24}O_{39.68}Ti_4Zr$
Formula weight	1276.43	1518.25
Crystal system	Tetragonal	Tetragonal
Space group	*I*4/*mmm*	*I*-42*m*
a/Å	14.3801(11)	16.496(3)
c/Å	26.976(2)	29.947(5)
Z	4	4
Temperature/K	298(2)	298(2)
Wavelength/Å	0.72768	0.72768
2θ range/ °	1.00 - 21.99	1.00 - 21.99
Number of reflections	160	225
Number of structural variables	58	66
R_p	0.03243	0.03840
R_{wp}	0.04954	0.05313
R_{exp}	0.03572	0.04694
GOF	1.387	1.132

Table S4. Atomic position difference of PCN-415 from refinement against ED and PXRD.

Atom	Difference (Å)
Zr1	0.049
Ti1	0.014
Average Zr, Ti	0.032
O1	0.063
O2	0.035
O3	0.060
O4	0.146
O5	0.075
C1	0.136
C2	0.088
C3	0.064
C4	0.036
C5	0.023
C6	0.073
C7	0.058
Average O, C	0.071

Table S5. SEM-EDX and ICP data for PCN-415 and -416

MOF	**PCN-415**	**PCN-416**
Theoretical Ti/Zr ratio	4	4
Ti/Zr ratio based on EDX	4.3	3.3
Ti/Zr ratio based on ICP	3.8	3.6

Table S6. Cycling experiments of photocatalytic H_2 generation reaction[a]

Cycle	**H_2 ($\mu mol \cdot g^{-1}$ h^{-1})**
1	495
2	465
3	513

[a]Reaction conditions: 5 mg catalyst, 28 mL CH_3CN, 2 mL TEOA, 200 μL H_2O, 50 μg Pt, 300 W Xe lamp with a UV cut-off filter (λ > 380 nm), 4 h. Cycling experiments were conducted by adding 2 mL TEOA as sacrificial reagent at the end of each reaction. The reaction mixture was purged with nitrogen for 60 min before the next reaction cycle.

Table S7. Comparison of different MOF photocatalyst for H_2 generation reaction[a]

MOFs	**H_2 ($\mu mol \cdot g^{-1}$ h^{-1})**
UiO-66-NH_2	94
PCN-415-NH_2	594
MIL-125-NH_2	1328

[a]Reaction conditions: 5 mg catalyst, 28 mL CH_3CN, 2 mL TEOA, 200 μL H_2O, 50 μg Pt, 300 W Xe lamp with a UV cut-off filter (λ > 380 nm), 4 h.

REFERENCES

(1) APEX2 v2012.2.0 and SAINT v7.68A data collection and data processing programs, respectively. Bruker Analytical X-ray Instruments, Inc., Madison, WI.

(2) SADABS v2008/1 semi-empirical absorption and beam correction program. Sheldrick, G. M. University of Göttingen, Germany.

(3) Sheldrick, G. M. SHELXL, Version 6.14, Structure Determination Software Suite, Bruker AXS, Madison, WI, 2003.

(4) Rees, B.; Jenner, L.; Yusupov, M., Bulk-solvent correction in large macromolecular structures. *Acta Crystallogr. D,* **2005**, *61* (9), 1299-1301.

(5) Kratzert, D.; Holstein, J. J.; Krossing, I., DSR: enhanced modelling and refinement of disordered structures with SHELXL. *J. Appl. Crystallogr.* **2015**, *48* (3), 933-938.

(6) Wan, W.; Sun, J.; Su, J.; Hovmoller, S.; Zou, X., Three-dimensional rotation electron diffraction: software RED for automated data collection and data processing. *J. Appl. Crystallogr.* **2013**, *46* (6), 1863-1873.

(7) Kabsch, W., Integration, scaling, space-group assignment and post-refinement. *Acta Crystallogr. D* **2010**, *66* (2), 133-144.

(8) Sheldrick, G., A short history of SHELX. *Acta Crystallogr. A* **2008**, *64* (1), 112-122.

(9) Rietveld, H., A profile refinement method for nuclear and magnetic structures. *J. Appl. Crystallogr.* **1969**, *2* (2), 65-71.

(10) Kresse, G.; Hafner, J., Ab initio. *Phys. Rev. B* **1993**, *47* (1), 558-561.

(11) Perdew, J. P.; Burke, K.; Ernzerhof, M., Generalized Gradient Approximation Made Simple. *Phys. Rev. Lett.* **1996**, *77* (18), 3865-3868.